Role of magnetic and atomic ordering in the martensitic transformation of Ni-Mn-In from a first-principles study

Chun-Mei Li,[1,*] Hu-Bin Luo,[1] Qing-Miao Hu,[1] Rui Yang,[1] Börje Johansson,[2,3,4] and Levente Vitos[2,3,5]

[1]*Shenyang National Laboratory for Materials Science, Institute of Metal Research, Chinese Academy of Sciences, 72 Wenhua Road, Shenyang 110016, China*

[2]*Applied Materials Physics, Department of Materials Science and Engineering, Royal Institute of Technology, Stockholm SE-100 44, Sweden*

[3]*Condensed Matter Theory Group, Physics Department, Uppsala University, P.O. Box 516, SE-75120 Uppsala, Sweden*

[4]*School of Physics and Optoelectronic Technology & College of Advanced Science and Technology Dalian University of Technology, Dalian 116024, China*

[5]*Research Institute for Solid State Physics and Optics, Budapest H-1525, P.O. Box 49, Hungary*

(Received 17 October 2012; revised manuscript received 27 November 2012; published 10 December 2012)

The composition-dependent lattice parameters, crystal structure, elastic properties, magnetic moment, and electronic structure of $Ni_2Mn_{1+x}In_{1-x}$ ($0 \leqslant x \leqslant 0.6$) are studied by using first-principles calculations. It is shown that the martensitic phase transition (MPT) from cubic $L2_1$ to tetragonal $L1_0$ accompanies the Mn_{Mn}-Mn_{In} ferromagnetic (FM) to antiferromagnetic (AFM) transition, at around the critical composition $x = 0.32$, in agreement with the experimental measurement. The Mn-In atomic disorder leads to decreasing stability of the martensite relative to the austenite, which depresses the MPT. The shear elastic constant C' of the parent phase first decreases slightly with increasing x and then remains almost unchanged above $x = 0.32$, indicating C' alone cannot account for the increase of the MPT temperature with x. The total magnetic moments for the $L2_1$ phase are in good agreement with those determined by experiments, whereas for the $L1_0$ phase they are slightly larger than the experimental data due to the possible Mn-In atomic disorder in the sample. The calculated density of states demonstrate that the covalent bonding between the minority spin states of Ni and In plays an important role in both the magnetic and structural stability.

DOI: 10.1103/PhysRevB.86.214205 PACS number(s): 62.20.fg, 31.15.es, 75.50.Cc, 64.70.kd

I. INTRODUCTION

X_2YZ Heusler alloys show martensitic phase transition (MPT) upon changing temperature. The MPT of these shape memory alloys is generally attributed to the lattice instability, as demonstrated by the soft phonon modes and the corresponding elastic constant, e.g., C' [$=1/2(C_{11} - C_{12})$].[1,2] The origin can be further traced to the Jahn-Teller distortion[3] and Fermi surface nesting[4] at electronic structure level.

Unlike the Ni-Mn-Ga family, Ni-Mn-Z (Z = In, Sn, Ge, and Sb) Heusler alloys undergo MPT only in the off-stoichiometric condition; e.g., the MPT was observed in $Ni_2Mn_{1+x}In_{1-x}$ only with x larger than about 0.32,[5,6] of which the origin is still to be uncovered. The Ni-Mn-In system near the Heusler composition shows marked differences in the magnetic properties from those of other Ni-Mn-based Heusler alloys. The major feature that particularly stands out is that the magnetization in the austenitic phase (cubic $L2_1$) increases with Mn content,[5–7] i.e., in $Ni_2Mn_{1+x}In_{1-x}$ the excess Mn-on-In sublattice (Mn_{In}) should be ferromagnetic (FM) instead of antiferromagnetic (AFM) coupling with that of the Mn-on-Mn site (Mn_{Mn}), as in $Ni_2Mn_{1+x}Ga_{1-x}$[8,9] and $Ni_2Mn_{1+x}Sn_{1-x}$.[10] However, the martensite (modulated or nonmodulated tetragonal structure) of $Ni_2Mn_{1+x}In_{1-x}$ possesses much smaller magnetic moment compared to its well defined FM parent phase,[6] and even to FM $L2_1$-Ni_2MnIn. In addition, similar to Ni-Mn-Sn[11] and Ni-Mn-Sb[12] systems, a large exchange bias (EB) has been experimentally found in the martensitic state of $Ni_{49.5}Mn_{34.5}In_{16}$ bulk polycrystal[13] which indicates that the FM and AFM states coexist in the system, and at the interfaces they couple each other. This reflects that in $Ni_2Mn_{1+x}In_{1-x}$ alloys the MPT may be accompanied by a complex rearrangement of the magnetic ordering. Nevertheless, at present, the true story of the magnetic state of the martensite still needs to be ascertained.

The magnetic property is closely related to the MPT in most of the shape memory alloys. For the Ni-Mn-Ga and Ni-Mn-Sn families, the decrease in the magnetization generally corresponds to the increase in the driving force for the structural phase transition, i.e., the raise of the MPT temperature (T_M).[14,15] In $Ni_2Mn_{1+x}In_{1-x}$, it is desirable to explore whether the abrupt drop of the magnetic moment from the austenite to martensite originates from the MPT itself. Besides, the Mn-Z type atomic disorder is easily formed in Ni-Mn-Z alloys, which is expected to have a great influence on the magnetic configuration of the systems, and consequently, maybe on the MPT. Experimentally, it has been reported that the thermodynamics of the MPT in $Ni_2Mn_{1+x}In_{1-x}$ is dominated by the atomic ordering because it influences the magnetic entropy during the process.[16] Therefore, the investigation in detail about the atomic ordering effect on the phase stability has great significance.

Here we have clarified the origin of the MPT from the magnetic and atomic ordering point of view for $Ni_2Mn_{1+x}In_{1-x}$ by using first-principles calculations, performed with an exact muffin-tin orbitals (EMTO) method in combination with a coherent potential approximation (CPA).[17–21] From our calculations, it is also uncovered why the experimental magnetic moment is much lower in the martensite than that in the austenite of $Ni_2Mn_{1+x}In_{1-x}$. The rest of the paper is arranged as follows: in Sec. II, we describe the employed first-principles method and the details of the calculations. In

Sec. III, the composition-dependent lattice parameters, crystal structure, elastic property, magnetic moment, and electronic structure are presented. The magnetic and atomic ordering effects on the MPT as well as their electronic origin are discussed. Finally, we summarize the main results of this work in Sec. IV.

II. METHODS AND CALCULATION DETAILS

Within the present EMTO program,[17–21] the one-electron Kohn-Sham equation is solved by the use of a Green's function technique. The effective potential is approximated with the optimized overlapping muffin-tin potential. The total energy is calculated with a full-charge density technique.[18,20] In addition, in combination with the CPA method,[18,21] the EMTO program is flexible enough to describe the random distribution of the different atoms on one sublattice, and also the random distribution of the local magnetic moments. In a number of former works, the accuracy of the EMTO-CPA method for the equation of state of metals and disordered alloys has been successfully demonstrated.[21–26] In the present application, most of the parameters are set as in Ref. 27. Nevertheless, in order to improve the precision of the calculation, 17 × 17 × 17 k-point mesh is adopted here throughout the calculations.

The crystal structure of the high-temperature $L2_1$-Ni_2MnIn is shown in Fig. 1(a). Ni atoms are located at the $(\frac{1}{4}, \frac{1}{4}, \frac{1}{4})$ and $(\frac{3}{4}, \frac{3}{4}, \frac{3}{4})$ sublattices, Mn atoms occupy the $(\frac{1}{2}, \frac{1}{2}, \frac{1}{2})$ sublattice, and In atoms occupy the (0, 0, 0) sublattice. Figure 1(b) depicts the crystal structure of the nonmodulated tetragonal martensite ($L1_0$). In the off-stoichiometric $Ni_2Mn_{1+x}In_{1-x}$ alloys, the excess Mn atoms prefer to occupy the In sublattice.[6] We assume that they are distributed randomly on the In sublattice, which is described within the framework of the CPA.[18,21] Similarly, for the Mn-In disordered phases with $Mn_{(1+x)/2}In_{(1-x)/2}$ on both Mn and In sublattices, the atomic disorder is treated also in the same way.

The equilibrium lattice parameter (a) and bulk modulus are determined by fitting the calculated total energies versus volume (nine data points) to a Morse function.[28] The shear elastic constants (C' and C_{44}) in cubic structure are calculated by the use of volume conserving orthorhombic and monoclinic deformations, which have been described clearly in our previous work.[29] The Ni $3d^8 4s^2$, Mn $3d^5 4s^2$, and In $3d^{10} 4s^2 4p^1$ are treated as valence electrons.

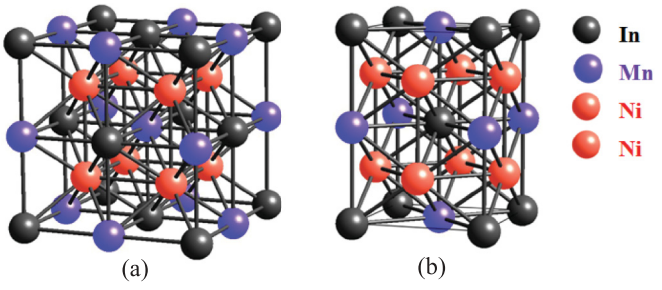

FIG. 1. (Color online) Unit cells of standard stoichiometric Ni_2MnIn with simple cubic $L2_1$ structure (a) and body-centered-tetragonal $L1_0$ structure (b) in the [1 1 0] direction.

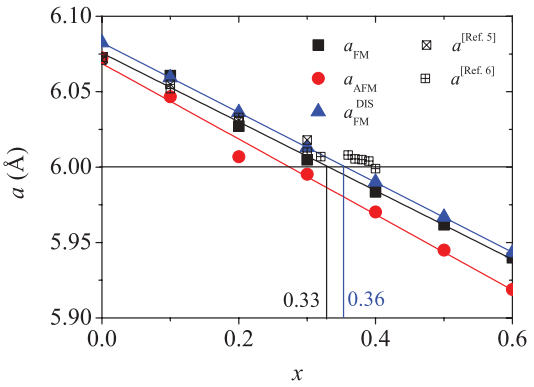

FIG. 2. (Color online) Theoretical lattice parameters of the ordered $L2_1$-$Ni_2Mn_{1+x}In_{1-x}$ ($0.0 \leqslant x \leqslant 0.6$) in FM ($a_{FM}$) and AFM ($a_{AFM}$) states as well as the disordered alloys in the FM state (a_{FM}^{DIS}), with respect to x, in comparison with the experimental data cited from Refs. 5 and 6 (denoted by $a^{[Ref.\ 5]}$ and $a^{[Ref.\ 6]}$, respectively).

III. RESULTS AND DISCUSSION

A. Lattice parameter of austenite

Figure 2 shows the composition-dependent equilibrium lattice parameters of the ordered $L2_1$-$Ni_2Mn_{1+x}In_{1-x}$ ($0 \leqslant x \leqslant 0.6$) in FM ($a_{FM}$) and AFM ($a_{AFM}$) states as well as the disordered alloys in the FM (a_{FM}^{DIS}) state. For Ni_2MnIn, our a_{FM} is about 6.072 Å, in good agreement with the experimental (6.071 Å[5]) and other theoretical values (6.090 Å[30] and 6.060 Å[31]). With increasing Mn excess (x), a_{FM}, a_{AFM}, and a_{FM}^{DIS} decrease linearly. At each composition, a_{AFM} is smaller than a_{FM}, whereas a_{FM}^{DIS} is slightly larger than a_{FM}. Within the whole range of the studied off-stoichiometric composition, a_{FM} is in better agreement with the available experimental data[5,6] than a_{AFM}. However, for $0.3 \leqslant x \leqslant 0.4$, a_{FM}^{DIS} seems to be closer to the experimental lattice parameter[6] than a_{FM}. Experimentally, it has been found that when x rises up to 0.36, the $Ni_2Mn_{1+x}In_{1-x}$ alloy exhibits B_2 structure instead of $L2_1$ at room temperature.[5] This indicates that, when $x \geqslant 0.3$, the Mn-In disordered state with relatively little higher electronic total energy may be stabilized by temperature effects or dynamic factors at finite temperature.

Based on the experimental measurements, there is a roughly established assumption that the MPT of the shape memory alloys occurs in alloys having austenitic lattice parameter of less than 6.0 Å.[32] From our calculations, this critical lattice parameter corresponds to the critical composition of $x = 0.33$ for the FM $L2_1$ ordered phase and $x = 0.36$ for the FM $L2_1$ disordered one (as shown in Fig. 2). The theoretical critical compositions are in reasonable agreement with the experimental data ranging from 0.368 to 0.38.[5,6] In addition, it is expected that the atomic disorder tends to expand the volume and depress the occurrence of the MPT, which follows its referred volume effect in Refs. 32–34; i.e., the expansion of the volume in the cubic phase corresponds to the decrease of the T_M.

B. Martensitic phase

In the present work, we focus ourselves on nonmodulated tetragonal martensite with $L1_0$ structure. In order to determine

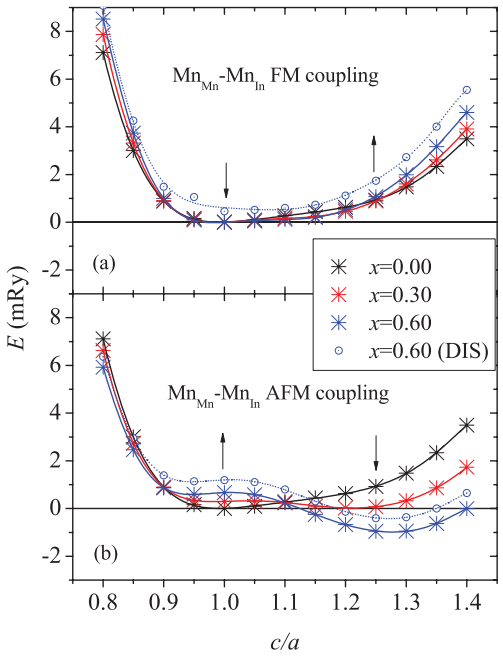

FIG. 3. (Color online) The total energy change with respect to c/a in $Ni_2Mn_{1+x}In_{1-x}$ ($x = 0.0$, 0.3, and 0.6) with Mn_{Mn} and Mn_{In} FM coupling (a) and AFM coupling (b). For comparison, the corresponding theoretical result for the disordered system with $x = 0.6$ is also shown. The reference state is the ordered FM cubic phase ($c/a = 1$).

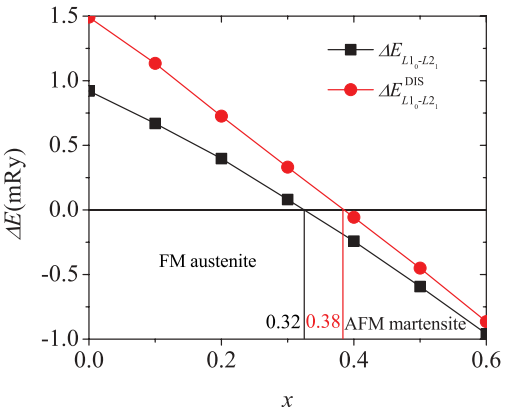

FIG. 4. (Color online) The energy difference between AFM $L1_0$ ($c/a = 1.25$) and FM $L2_1$ ($c/a = 1$) ordered ($\Delta E_{L1_0-L2_1}$) as well as disordered ($\Delta E^{DIS}_{L1_0-L2_1}$) $Ni_2Mn_{1+x}In_{1-x}$ ($0 \leqslant x \leqslant 0.6$) with respect to x.

the equilibrium state of the phase, we calculate the total energy against c/a with an interval of 0.05 for x from 0 to 0.6 with an interval of 0.1. Figure 3 shows the $E \sim c/a$ profiles for $x = 0.0$, 0.3, and 0.6. Here, the total energy at the FM $L2_1$ phase is treated as the reference energy. As seen in Fig. 3(a), with FM coupling between Mn_{In} and Mn_{Mn}, the $L2_1$ phase with $c/a = 1$ possesses the lowest energy for all three compositions without stable martensite being found. Figure 3(b) presents the energy profile with AFM coupling between Mn_{In} and Mn_{Mn}. For $x = 0.0$, the cubic phase with $c/a = 1$ is still globally stable. With increasing Mn excess, another energy minimum appears at $c/a > 1$, indicating that the $L1_0$ martensite becomes more stable than the AFM cubic phase. For $x = 0.3$, the AFM $E \sim c/a$ profile exhibits an energy minimum at about $c/a \approx 1.21$. This minimum is, however, slightly higher in energy (0.02 mRy) than the FM cubic phase. Therefore, the MPT may not occur with $x < 0.3$ since the FM cubic phase is the ground state in this case. With $x = 0.6$, we find an energy minimum at $c/a \approx 1.27$ corresponding to the AFM $L1_0$ phase. This phase is lower in energy than both AFM and FM cubic phases. Therefore, the MPT is expected.

The $E \sim c/a$ profiles of the disordered alloy with $x = 0.6$ are also included in Fig. 3. It is shown that, at each c/a value, the disordered system is higher in energy than the ordered one in both FM [Fig. 3(a)] and AFM states [Fig. 3(b)]. Similar to the ordered system, for the FM state [Fig. 3(a)], no martensite with $c/a > 1$ is found. For the AFM state [Fig. 3(b)], we again observe an energy minimum at $c/a \sim 1.25$ corresponding to the martensite.

As discussed above, when the MPT occurs, the off-stoichiometric $Ni_2Mn_{1+x}In_{1-x}$ cannot go directly from FM austenite to FM martensite. There must be a FM-to-AFM magnetic transition accompanying the MPT such that the AFM martensite can result. Such a magnetic transition at MPT temperature, the so-called metamagnetic transition, has been observed experimentally.[35,36]

Figure 3 clearly shows that the MPT of $Ni_2Mn_{1+x}In_{1-x}$ is composition and magnetic-state dependent. In order to get the critical composition at which the MPT occurs, we plot the energy difference between AFM $L1_0$ ($c/a = 1.25$) and FM $L2_1$ ($c/a = 1$) phases ($\Delta E_{L1_0-L2_1}$) as a function of x in Fig. 4. With increasing x, $\Delta E_{L1_0-L2_1}$ decreases almost linearly, indicating the stability of the AFM $L1_0$ phase relative to the FM $L2_1$ austenite increases. Around $x = 0.32$, it changes from positive to negative, i.e., the AFM $L1_0$ phase becomes more stable than the FM $L2_1$ phase. This means that, if we neglect the temperature effect on the free energy difference between the two phases, the critical composition for MPT in $Ni_2Mn_{1+x}In_{1-x}$ is about 0.32, close to the values (0.368[6] and 0.38[5]) determined by experimental measurements.

Also plotted in Fig. 4 is the energy difference between the $L1_0$ phase with $c/a = 1.25$ and the $L2_1$ phase of the disordered $Ni_2Mn_{1+x}In_{1-x}$ ($\Delta E^{DIS}_{L1_0-L2_1}$). The critical composition x of the MPT corresponding to $\Delta E^{DIS}_{L1_0-L2_1} = 0$ is about 0.38, higher than that for the ordered system. Moreover, for each composition, $\Delta E^{DIS}_{L1_0-L2_1}$ is larger than $\Delta E_{L1_0-L2_1}$, indicating that the atomic disorder increases the stability of the $L2_1$ cubic phase relative to the $L1_0$ martensitic phase. Similar to Ni-Mn-Ga alloys,[37] the MPT in the disordered $Ni_2Mn_{1+x}In_{1-x}$ is depressed to occur at relatively lower temperature.

In Table I, the lattice parameters of the ordered (a and c/a) and disordered (a^{DIS} and c/a^{DIS}) martensitic phases of $Ni_2Mn_{1+x}In_{1-x}$ ($x = 0.4$, 0.5, and 0.6) are listed. Similar to the cubic parent phase, both a and a^{DIS} in the martensite decrease with increasing x. At each composition, the atomic disorder enlarge a slightly. Nevertheless, with increasing Mn excess x, both c/a and c/a^{DIS} increase, and they are close to each other at the same composition. Experimentally, the Mn excess accelerates the occurrence of the MPT and increases T_M.[5] This suggests that, for $Ni_2Mn_{1+x}In_{1-x}$, a larger tetragonality of the

TABLE I. Theoretical equilibrium lattice parameters of the ordered [$a(x)$ in Å and $c/a(x)$] and disordered [$a^{\mathrm{DIS}}(x)$ in Å and $c/a^{\mathrm{DIS}}(x)$] martensitic $Ni_2Mn_{1+x}In_{1-x}$ ($x = 0.4$, 0.5, and 0.6).

x	$a(x)$	$c/a(x)$	$a^{\mathrm{DIS}}(x)$	$c/a^{\mathrm{DIS}}(x)$
0.4	5.9584	1.239	5.9623	1.240
0.5	5.9281	1.264	5.9317	1.256
0.6	5.8971	1.279	5.9002	1.276

martensite ($|c/a - 1|$) corresponds to a higher T_M, which is also found for Ni-Mn-Ga based alloys.[38,39]

C. Elastic property

The structural phase transition of alloys comes directly from the instability of the thermodynamical properties in the parent phase. For Ni-Mn-Ga shape memory alloys, the MPT is generally accompanied by the soft-phonon modes and the soft shear elastic constant C' of the high-temperature $L2_1$ phase.[1,2,40] In addition, the alloying effect on the MPT temperature T_M has been related to the composition-dependent C': a lower C' corresponding to a higher T_M in most of the off-stoichiometric alloys.[40–42] In order to better understand the mechanical stability of $Ni_2Mn_{1+x}In_{1-x}$ alloys, in this section we investigate the composition-dependent elastic constants of the FM cubic phase.

In Fig. 5, the shear elastic constants (C' and C_{44}) and the anisotropic ratio ($A = C'/C_{44}$) are presented as functions of x. C', C_{44}, and A of the standard stoichiometric Ni_2MnIn are 12.10 ± 0.25 GPa, 106.81 ± 1.35 GPa, and 8.83, respectively, in good agreement with those from experimental measurements (12 ± 4 GPa, 90 ± 15 GPa, and 7.5, respectively[43]) and other first-principle calculations (15 GPa, 101 GPa, and 6.7, respectively[31]). In the range of $x \leqslant 0.3$, with increasing x (or e/a), C' becomes gradually softer but C_{44} gets stiffer, which results in larger A. However, when the Mn excess exceeds 0.3, C', C_{44}, and A keep almost constant against x although the experimental T_M increases with x. This result suggests that, unlike Ni-Mn-Ga, the composition-dependent elastic properties alone are not sufficient to account for the variation of T_M against x for $Ni_2Mn_{1+x}In_{1-x}$ ($x > 0.3$). For this system, the properties of the martensite (e.g., its stability relative to the austenite) have to be taken into account in order to understand the composition-dependent T_M as discussed in the previous subsection.

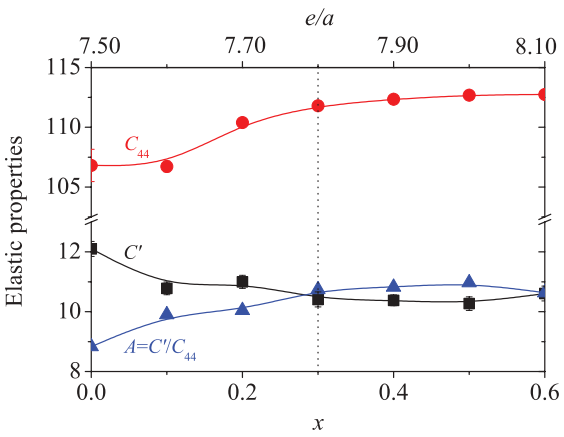

FIG. 5. (Color online) The shear elastic constants (C' and C_{44}, in GPa) and the anisotropic ratio ($A = C'/C_{44}$) of the FM $L2_1$-$Ni_2Mn_{1+x}In_{1-x}$ ($0.0 \leqslant x \leqslant 0.6$) with respect to x as well as the number of valence electrons per atom (e/a).

D. Magnetic moment

Similar to other Ni-Mn-Z (Z = Ga, Sn, and Sb) Heusler alloys,[44] the total magnetic moment (μ_{tot}) of $Ni_2Mn_{1+x}In_{1-x}$ is mainly localized on the Mn atoms with a small contribution from the Ni atoms. The magnetic moment of In, depending on the composition of the alloy, is merely $0.02\mu_B$–$0.05\mu_B$. For the FM standard stoichiometric Ni_2MnIn, Ni and Mn atoms possess magnetic moments of $0.29\mu_B$ and $3.59\mu_B$, respectively. μ_{tot} is around $4.13\mu_B$, in good agreement with experimental measurements ($4.1\mu_B$[6]) and other first-principles calculations ($4.208\mu_B$[44] and $4.41\mu_B$[30]).

The variation of the total magnetic moment μ_{tot} with respect to x is shown in Fig. 6. For the cubic $L2_1$ phase with Mn_{In} ferromagnetically coupled with Mn_{Mn}, the total magnetic moment ($\mu_{\mathrm{tot}}^{L2_{1\mathrm{FM}}}$) increases linearly with x. On the other hand, for the $L1_0$ phase with Mn_{In} antiferromagnetically coupled with Mn_{Mn}, the total magnetic moment ($\mu_{\mathrm{tot}}^{L1_{0\mathrm{AFM}}}$) decreases linearly with increasing x. For $x < 0.32$, $\mu_{\mathrm{tot}}^{L2_{1\mathrm{FM}}}$ is in good agreement with the experimental magnetic moments of the austenite ($\mu_{\mathrm{tot}}^{L2_1\,[\mathrm{Ref.\ 6}]}$), whereas for $x > 0.36$ the trend of $\mu_{\mathrm{tot}}^{L1_{0\mathrm{AFM}}}$ is consistent with that of the experimental magnetic moments of the martensite ($\mu_{\mathrm{tot}}^{L1_0\,[\mathrm{Ref.\ 6}]}$). This again demonstrates the coupling between the metamagnetic and the structural transition of $Ni_2Mn_{1+x}In_{1-x}$, noting that the critical composition for the structure transition is $x \sim 0.32$.

For the disordered FM $L2_1$ phase, the total magnetic moment ($\mu_{\mathrm{tot}}^{L2_{1\mathrm{FM}}^{\mathrm{DIS}}}$) is almost the same as $\mu_{\mathrm{tot}}^{L2_{1\mathrm{FM}}}$ at each composition x. This is because the ferromgnetically coupled Mn_{Mn} and Mn_{In} in the $L2_1$ phase have almost the same magnetic

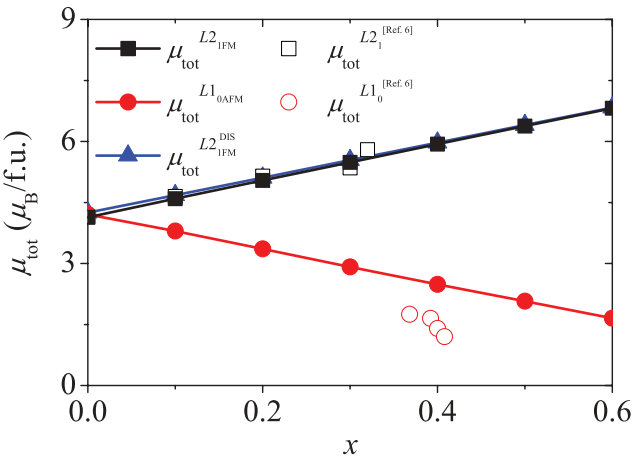

FIG. 6. (Color online) The composition dependence of the total magnetic moment in FM $L2_1$ ($\mu_{\mathrm{tot}}^{L2_{1\mathrm{FM}}}$) and AFM $L1_0$ ($\mu_{\mathrm{tot}}^{L1_{0\mathrm{AFM}}}$) ordered, and FM $L2_1$ disordered ($\mu_{\mathrm{tot}}^{L2_{1\mathrm{FM}}^{\mathrm{DIS}}}$) $Ni_2Mn_{1+x}In_{1-x}$ ($0 \leqslant x \leqslant 0.6$), in comparison with those of the experimental data in the two phases ($\mu_{\mathrm{tot}}^{L2_1\,[\mathrm{Ref.\ 6}]}$ and $\mu_{\mathrm{tot}}^{L1_0\,[\mathrm{Ref.\ 6}]}$, respectively).

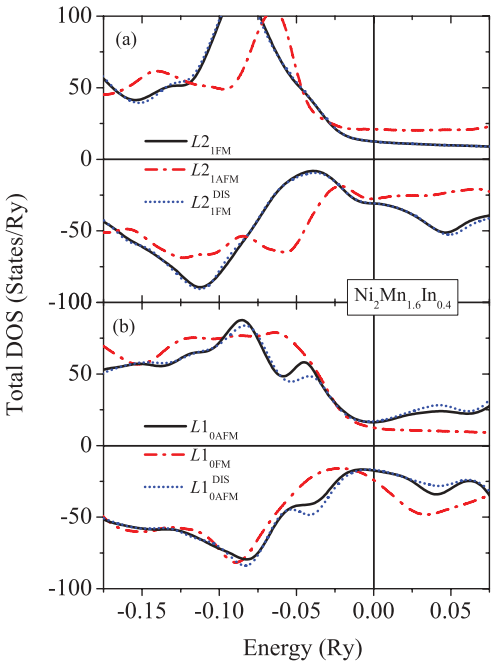

FIG. 7. (Color online) The total density of states (DOS) of $L2_1$-$Ni_2Mn_{1.6}In_{0.4}$ in FM ($L2_{1FM}$), AFM ($L2_{1AFM}$), and FM disordered ($L2_{1FM}^{DIS}$) states (a), as well as those of the $L1_0$ system in AFM ($L1_{0AFM}$), FM ($L1_{0FM}$), and AFM disordered ($L1_{0AFM}^{DIS}$) states (b). The vertical lines indicate the Fermi level.

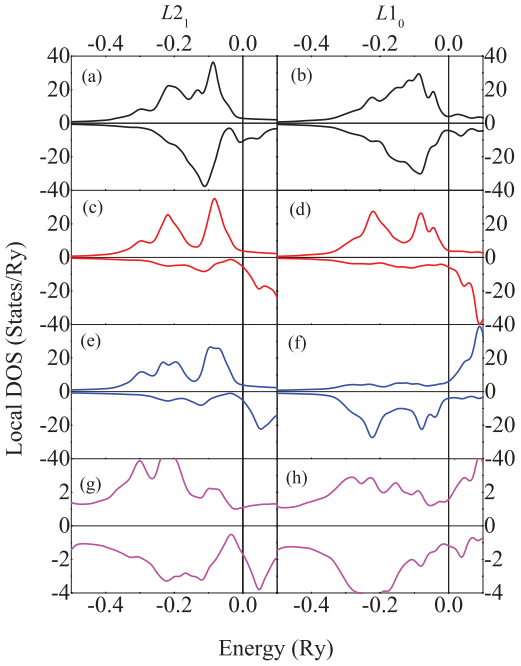

FIG. 8. (Color online) The local density of states (DOS) of Ni (panels a and b), Mn (panels c and d) on Mn sublattice, Mn (panels e and f) on In sublattice; and In (panels g and h) of $Ni_2Mn_{0.6}In_{0.4}$ in FM $L2_1$ (panels a, c, e and g) and AFM $L1_0$ (panels b, d, f, and h). The vertical lines indicate the Fermi level.

moments. When Mn_{Mn} and Mn_{In} are antiferromagnetically coupled, the total magnetic moments of the disordered FM $L2_1$ and AFM $L1_0$ phases are close to zero since Mn_{Mn} and Mn_{In} have the same atomic fraction. As seen in Fig. 6, the calculated total magnetic moment of the AFM $L1_0$ phase $\mu_{tot}^{L1_{0AFM}}$ is larger than those from the experiment measurement $\mu_{tot}^{L1_0}$[Ref. 6]. This indicates that there exists Mn-In disordering in the sample used in the experiment which decreases the total magnetic moment.

E. Electronic structure

In order to explore the electronic origin of the preference of the magnetic state and the MPT of $Ni_2Mn_{1+x}In_{1-x}$ alloys, we calculate the total density of states (DOS) of austenitic and martensitic $Ni_2Mn_{1.6}In_{0.4}$ at both FM and AFM states, as shown in Figs. 7(a) and 7(b), respectively. Here, the atomic disorder effect is also in consideration.

For the $L2_1$ phase [Fig. 7(a)], as compared to the FM state, the dominated peak around -0.075 Ry in the spin-up DOS shifts to higher energy at AFM state. The pseudogap around -0.05Ry in the spin-down DOS is much wider and deeper for the FM state than that for the AFM one, indicating that the covalent bonding of the FM state is stronger than that of the AFM phase in the view of the reported theory.[45–49] This accounts well for the more stable FM $L2_1$ phase compared to that of the AFM one.

For the $L1_0$ phase [Fig. 7(b)], in the AFM state, the Fermi level is located at the valley of the pseudogap, which means that the bonding states are fully occupied but the antibonding states are empty. In the FM state, some of the antibonding states are occupied by electrons. In addition, the peak of the spin-up DOS at around -0.06 Ry for the FM state splits for the AFM state. Both the band-filling effect and the spliting of the spin-up peak at -0.06 Ry make the AFM state more stable than the FM one.

In Figs. 7(a) and 7(b), we note that the total DOS in the ordered and disordered $Ni_2Mn_{1.6}In_{0.4}$ are not very different from each other for the two phases, which may provide a good explanation for the existence of the atomic disorder in the alloy.

Figure 8 shows the local DOSs of Ni [(a) and (b)], Mn_{Mn} [(c) and (d)], Mn_{In} [(e) and (f)], and In [(g) and (h)] of $Ni_2Mn_{0.6}In_{0.4}$ in FM $L2_1$ and AFM $L1_0$ phases. In comparison, the resonance between the minority electronic states of Ni and In around the pseudogap is more significant than that between Mn_{Mn} (or Mn_{In}) and In, especially in the AFM $L1_0$ phase, indicating that the covalent bond is mainly formed due to the hybridization between the minority electronic states of Ni and In. This is understandable since Ni atom is the nearest neighbor whereas Mn_{Mn} and Mn_{In} are the second- and third-nearest neighbors, respectively, of In and, therefore, the interaction between Ni and In is expected to be stronger than that between Mn_{Mn} and In as well as Mn_{In} and In.

To explore the physics behind the composition-dependent MPT, we compare the total DOS of both the FM $L2_1$ and the AFM $L1_0$ phases of $Ni_2Mn_{1+x}In_{1-x}$ with $x = 0$, 0.3, and 0.6 as shown in Fig. 9. For the FM $L2_1$ phase of each alloy, the Fermi level is located at the antibonding states as shown by a small peak (the upper bound of the pseudogap at around -0.05) at the Fermi level, which decreases the stability of the phase at low temperature. This small peak splits when the FM $L2_1$ phase transforms to the AFM $L1_0$ phase, which locates

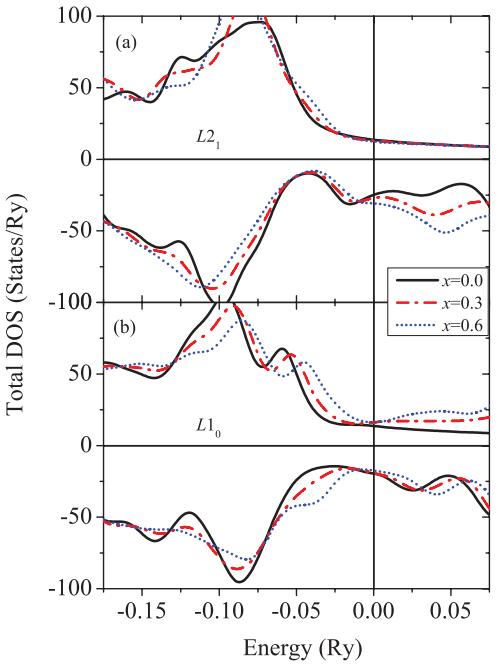

FIG. 9. (Color online) The total density of states (DOS) of (a) FM $L2_1$- and (b) AFM $L1_0$-$Ni_2Mn_{1+x}In_{1-x}$ ($x = 0.0$, 0.3, and 0.6). The vertical lines indicate the Fermi level.

the Fermi level of the AFM $L1_0$ phase right at the valley of the pseudogap. This is so called Jahn-Teller splitting effect[3] and makes the AFM $L1_0$ phase more stable than the $L2_1$ phase at low temperature.

For the FM $L2_1$ phase [Fig. 9(a)], the width of the pseudogap around -0.05 Ry of the minority DOS increases slightly with increasing x, indicating that the covalent bond becomes slightly stronger and the stability of the $L2_1$ phase increases accordingly. For the $L1_0$ phase [Fig. 9(b)], the pseudogap moves up in energy with increasing x and the Fermi level moves to the valley of the pseudogap, resulting in less antibonding states occupied by electrons. Therefore, the stability of the $L1_0$ phase increases with x as well. The increasing T_M with x might be due to the fact that the stability of the $L1_0$ phase increases faster than that of the $L2_1$ phase.

IV. SUMMARY

Using the first-principles EMTO-CPA method, we have investigated the composition dependence of the lattice parameters, crystal structure, elastic properties, magnetic moment, and electronic structure of $Ni_2Mn_{1+x}In_{1-x}$ ($0 \leqslant x \leqslant 0.6$) alloys. The main results are summarized as follows:

(1) The Mn atoms on Mn sublattice (Mn_{Mn}) are ferromagnetically coupled with the Mn atoms on In sublattice (Mn_{In}) for the $L2_1$ austenite, whereas for the $L1_0$ martensite they are antiferromagnetically coupled, indicating that the martensitic transition occurs with the accompanying FM-AFM transition.

(2) The energy difference between the AFM $L1_0$ phase and the FM $L2_1$ phase decreases linearly with increasing x. With x smaller than 0.32, the FM $L2_1$ phase is more stable than the AFM $L1_0$ phase, and, therefore, the MPT cannot occur. With x larger than about 0.32, the FM $L2_1$ phase is less stable than the AFM $L1_0$ phase such that the MPT is expected. The theoretical critical composition x of about 0.32 for the MPT is in good agreement with the experimental measurement. The Mn-In disordering leads to decreasing stability of the martensite relative to the austenite, which may depress the MPT.

(3) With x smaller than about 0.32, C' of the FM $L2_1$ phase decreases slightly with increasing x. However, C' remains almost unchanged with further increasing x. The composition-dependent C' of the $L2_1$ phase alone may not account for the variation of the MPT temperature against x for $Ni_2Mn_{1+x}In_{1-x}$ alloy.

(4) The theoretical total magnetic moment of the $L2_1$ phase with $x < 0.32$ is in good agreement with that determined by experiments. The trend of the magnetic moment of the $L1_0$ phase against x agrees well with the experimental finding but with smaller absolute value due to the possible Mn-In atomic disordering in the sample used in the experiments.

(5) The calculated electronic structure shows that the covalent bonding between the minority spin states of atoms plays an important role in both the magnetic and structural stability.

ACKNOWLEDGMENTS

The authors acknowledge financial support from the MoST of China under Grant No. 2011CB606404 and the NSFC under Grant No. 50871114. The Swedish Research Council, the Swedish Steel Producers' Association, and the Hungarian Scientific Research Fund (research project OTKA 84078) are acknowledged for financial support. C.-M.L. is also grateful to the T. S. Kê Research Fellowship of IMR/SYNL.

*Corresponding author: cmli@imr.ac.cn

[1] C. Bungaro, K. M. Rabe, and A. Dal Corso, Phys. Rev. B **68**, 134104 (2003).
[2] M. Wutting, L. H. Liu, K. Tsuchiya, and R. D. James, J. Appl. Phys. **87**, 4707 (2000).
[3] S. Fujii, S. Ishida, and S. Asano, J. Phys. Soc. Jpn. **58**, 3657 (1989).
[4] C. P. Opeil, B. Mihaila, R. K. Schulze, L. Mañosa, A. Planes, W. L. Hults, R. A. Fisher, P. S. Riseborough, P. B. Littlewood, J. L. Smith, and J. C. Lashley, Phys. Rev. Lett. **100**, 165703 (2008).
[5] T. Krenke, M. Acet, E. F. Wassermann, X. Moya, L. Mañosa, and A. Planes, Phys. Rev. B **73**, 174413 (2006).
[6] T. Kanomata, T. Yasuda, S. Sasaki, H. Nishihara, R. Kainuma, W. Ito, K. Oikawa, K. Ishida, K. U. Neumann, and K. R. A. Ziebeck, J. Magn. Magn. Mater. **321**, 773 (2009).
[7] T. Miyamoto, W. Ito, R. Y. Umetsu, R. Kainuma, T. Kanomata, and K. Ishida, Scr. Mater. **62**, 151 (2010).
[8] Q. M. Hu, C. M. Li, S. E. Kulkova, R. Yang, B. Johansson, and L. Vitos, Phys. Rev. B **81**, 064108 (2010).

[9]J. Enkovaara, O. Heczko, A. Ayuela, and R. M. Nieminen, Phys. Rev. B **67**, 212405 (2003).
[10]M. Ye, A. Kimura, Y. Miura, M. Shirai, Y. T. Cui, K. Shimada, H. Namatame, M. Taniguchi, S. Ueda, K. Kobayashi, R. Kainuma, T. Shishido, K. Fukushima, and T. Kanomata, Phys. Rev. Lett. **104**, 176401 (2010).
[11]M. Khan, I. Dubenko, S. Stadler, and N. Ali, Appl. Phys. Lett. **91**, 072510 (2007).
[12]Z. Li, C. Jing, J. P. Chen, S. J. Yuan, S. X. Cao, and J. C. Zhang, Appl. Phys. Lett. **91**, 112505 (2007).
[13]B. M. Wang, Y. Liu, L. Wang, S. L. Huang, Y. Zhao, Y. Yang, and H. Zhang, J. Appl. Phys. **104**, 043916 (2008).
[14]T. Krenke, M. Acet, E. F. Wassermann, X. Moya, L. Mañosa, and A. Planes, Phys. Rev. B **72**, 014412 (2005).
[15]V. V. Khovaylo, V. D. Buchelnikov, R. Kainuma, V. V. Koledov, M. Ohtsuka, V. G. Shavrov, T. Takagi, S. V. Taskaev, and A. N. Vasiliev, Phys. Rev. B **72**, 224408 (2005).
[16]V. Recarte, J. I. Pérez-Landazábal, V. Sánchez-Alarcos, and J. A. Rodríguez-Velamazán, Acta Mater. **60**, 1937 (2012).
[17]L. Vitos, Phys. Rev. B **64**, 014107 (2001).
[18]L. Vitos, *Computational Quantum Mechanics for Materials Engineers* (Springer-Verlag, London, 2007).
[19]O. K. Andersen, O. Jepsen, and G. Krier, in *Lectures on Methods of Electronic Structure Calculations*, edited by V. Kumar, O. K. Andersen, and A. Mookerjee (World Scientific, Singapore, 1994), pp. 63–124.
[20]J. Kollár, L. Vitos, and H. L. Skriver, in *Electronic Structure and Physical Properties of Solids: The Uses of the LMTO Method*, Lectures Notes in Physics, edited by H. Dreyssé (Springer-Verlag, Berlin, 2000), p. 85.
[21]L. Vitos, I. A. Abrikosov, and B. Johansson, Phys. Rev. Lett. **87**, 156401 (2001).
[22]B. L. Gyorffy, Phys. Rev. B **5**, 2382 (1972).
[23]A. Taga, L. Vitos, B. Johansson, and G. Grimvall, Phys. Rev. B **71**, 014201 (2005).
[24]B. Magyari-Köpe, G. Grimvall, and L. Vitos, Phys. Rev. B **66**, 064210 (2002); **66**, 179902(E) (2002).
[25]L. Vitos, P. A. Korzhavyi, and B. Johansson, Phys. Rev. Lett. **88**, 155501 (2002).
[26]L. Vitos, P. A. Korzhavyi, and B. Johansson, Nat. Mater. **2**, 25 (2003).
[27]C. M. Li, H. B. Luo, Q. M. Hu, R. Yang, B. Johansson, and L. Vitos, Phys. Rev. B **84**, 174117 (2011).
[28]V. L. Moruzzi, J. F. Janak, and K. Schwarz, Phys. Rev. B **37**, 790 (1988).
[29]C. M. Li, Q. M. Hu, R. Yang, B. Johansson, and L. Vitos, Phys. Rev. B **82**, 094201 (2010).
[30]S. Ağduk and G. Gökoğlu, Eur. Phys. J. B **79**, 509 (2011).
[31]A. T. Zayak, P. Entel, K. M. Rabe, W. A. Adeagbo, and M. Acet, Phys. Rev. B **72**, 054113 (2005).
[32]A. Planes, L. Mañosa, and M. Acet, J. Phys.: Condens. Matter **21**, 233201 (2009).
[33]Y. Xin, Y. Li, C. B. Jiang, and H. B. Xu, Mater. Sci. Forum **475–479**, 1991 (2005).
[34]V. V. Kokorin, I. A. Osipenko, and T. V. Shirina, Phys. Met. Metallogr. **67**, 173 (1989).
[35]T. Krenke, E. Duman, M. Acet, E. F. Wassermann, X. Moya, L. Mañosa, and A. Planes, Nat. Mater. **4**, 450 (2005).
[36]K. Oikawa, W. Ito, Y. Imano, Y. Sutou, R. Kainuma, and K. Ishida, Appl. Phys. Lett. **88**, 122507 (2006).
[37]V. Sánchez-Alarcos, V. Recarte, J. I. Pérez-Landazábal, and G. J. Cuello, Acta Mater. **55**, 3883 (2007).
[38]N. Lanska, O. Söderberg, A. Sozinov, Y. Ge, K. Ullakko, and V. K. Lindroos, J. Appl. Phys. **95**, 8074 (2004).
[39]S. Banik, R. Ranjan, A. Chakrabarti, S. Bhardwaj, N. P. Lalla, A. M. Awasthi, V. Sathe, D. M. Phase, P. K. Mukhopadhyay, D. Pandey, and S. R. Barman, Phys. Rev. B **75**, 104107 (2007).
[40]M. Stipcich, L. Mañosa, A. Planes, M. Morin, J. Zarestky, T. Lograsso, and C. Stassis, Phys. Rev. B **70**, 054115 (2004).
[41]Q. M. Hu, C. M. Li, R. Yang, S. E. Kulkova, D. I. Bazhanov, B. Johansson, and L. Vitos, Phys. Rev. B **79**, 144112 (2009).
[42]C. M. Li, H. B. Luo, Q. M. Hu, R. Yang, B. Johansson, and L. Vitos, Phys. Rev. B **82**, 024201 (2010).
[43]X. Moya, D. González-Alonso, L. Mañosa, A. Planes, V. O. Garlea, T. A. Lograsso, D. L. Schlagel, J. L. Zarestky, S. Aksoy, and M. Acet, Phys. Rev. B **79**, 214118 (2009).
[44]E. Şaşioglu, L. M. Sandratskii, and P. Bruno, Phys. Rev. B **70**, 024427 (2004).
[45]C. D. Gelatt, Jr., A. R. Williams, and V. L. Moruzzi, Phys. Rev. B **27**, 2005 (1983).
[46]J.-H. Xu, T. Oguchi, and A. J. Freeman, Phys. Rev. B **35**, 6940 (1987).
[47]J.-H. Xu, T. Oguchi, and A. J. Freeman, Phys. Rev. B **36**, 4186 (1987).
[48]Q. M. Hu, R. Yang, D. S. Xu, Y. L. Hao, D. Li, and W. T. Wu, Phys. Rev. B **68**, 054102 (2003).
[49]T. Hong, T. J. Watson-Yang, A. J. Freeman, T. Oguchi, and J. H. Xu, Phys. Rev. B **41**, 12462 (1990).